Langmuir Article

pubs.acs.org/Langmuir

One-Step Dry Method for the Synthesis of Supported Single-Crystalline Organic Nanowires Formed by π-Conjugated Molecules

Ana Borras,*[,†,‡] Oliver Gröning,[†] Myriam Aguirre,[§] Fabian Gramm,[⊥] and Pierangelo Gröning[†]

[†]*Empa, Swiss Federal Laboratories for Materials Testing and Research: "Nanotech@surfaces" Laboratory, Feuerwerkerstrasse 39, CH-3602 Thun, Switzerland,* [‡]*Institute of Materials Science of Seville (CSIC-U. Sevilla): Surfaces, Interfaces and Thin Films Laboratory, Avd. Americo Vespucio 49, 41092 Seville, Spain,* [§]*EMPA: "Solid State Chemistry and Analysis" Laboratory, Uberlandstrasse 129, CH-8600 Dübendorf, Switzerland, and* [⊥]*Electron Microscopy ETH Zurich (EMEZ), Wolgang-Pauli-Str. 16, 8093 Zurich, Switzerland*

Received September 17, 2009. Revised Manuscript Received March 8, 2010

We present for the first time a general vacuum process for the growth of supported organic nanowires formed by π-conjugated molecules, including metalloporphyrins, metallophthalocyanines, and perylenes. This methodology consists on a one-step physical vapor deposition of the π-conjugated molecules. The synthesis is carried out at controlled temperature on substrates with tailor morphology which allows the growth of organic nanowires in the form of squared nanofibers and nanobelts. The study of the nanowires by electron diffraction and HRTEM combining with the results of a theoretical analysis of the possible arrangement of the π-conjugated molecules along the nanowires reveals that the nanowires show a columnar structure along the fiber axis consisting of π-stacked molecules having a herringbone-like arrangement. The formation of these nanowires on different substrates demonstrates that the growth mechanism is independent of the substrate chemical composition. An in-depth phenomenological study of the formation of the nanowires drives us to propose a growth mechanism based on a crystallization process. Furthermore, the growth method allows the fabrication of two particular 1D heterostructures: binary and open core@shell organic nanofibers.

Introduction

Functional one-dimensional (1D) materials are of great interest for their use in nanoscale optical and electronic devices. During recent years the use of π-conjugated molecules as building blocks for organic nanostructures has received special attention and interest.[1] The intramolecular delocalized π-electron system, responsible for the characteristic stacking of these molecules, with its high polarizability plays a key role in defining their remarkable conductive, magnetic, and optical properties.[1b] Among the class of π-conjugated molecules, the families of metalloporphyrins and phthalocyanines are promising materials in applications such as vapor (gas) nanosensors and as active components for photonic devices, organic field effect transistors (OFETs), phototransistors, and solar cells.[2] Different works have established that the perylene diimide (MePTCDI) and other materials of the perylene family are some of the few n-type organic semiconductors showing high charge carrier mobilities.[3] Because of that, they are excellent candidates for the formation of low-dimensional molecular electronic nanostructures.[3]

In general, three strategies for the growth of organic nanowires (ONWs) have been addressed: self-assembly via solution deposition,[1b,4] template methods,[5] and vapor transport process.[6] The use of techniques based on solution processes present different shortcomings when trying to control the size, morphology, or

*Corresponding author: Ph +34954489528; Fax +34954460665; e-mail anaisabel.borras@icmse.csic.es.

(1) (a) Schenning, A. P. H. J.; Meijer, E. W. *Chem. Commun.* **2005**, 3245. (b) Liu, H.; Li, Y.; Daoben, Z. *Int. J. Nanotechnol.* **2007**, *4*, 197. (c) Briseno, A. L.; Mannsfeld, S. C. B.; Jenekhe1, S. A.; Bao, Z.; Xia, Y. *Mater. Today* **2008**, *11*, 38. (d) Zhao, Y. S.; Peng, A.; Fu, H.; Ma, Y.; Yao, J. *Adv. Mater.* **2008**, *20*, 1661.

(2) (a) Claessens, C. G.; Hahn, U.; Torres, T. *Chem. Rec.* **2008**, *8*, 75. (b) Troshin, P. A.; Koeppe, R.; Peregudov, A. S.; Peregudova, S. M.; Egginger, M.; Lyubovskaya, R. N.; Sariciftci, N. S. *Chem. Mater.* **2007**, *19*, 5363. (c) Curtis, M. D.; Cao, J.; Kampf, J. W. *J. Am. Chem. Soc.* **2004**, *126*, 4318. (d) Wang, W.; Han, J. J.; Wang, L.-Q.; Li, L.-S.; Shaw, W. J.; Li, A. D. Q. *Nano Lett.* **2003**, *3*, 455. (e) Lee, J. W.; Kang, H.-S.; Kim, M.-K.; Kim, K.; Cho, M.-Y.; Kwon, Y.-W.; Jooa, J.; Kim, J.-I.; Hong, C.-S. *J. Appl. Phys.* **2007**, *102*, 124104. (f) Claessens, C. G.; Hahn, U.; Torres, T. *Chem. Rec.* **2008**, *8*, 75.

(3) (a) Dimitrakopoulos, C. D.; Malenfant, P. R. L. *Adv. Mater.* **2002**, *14*, 99. (b) Van der Boom, T.; Hayes, R. T.; Zhao, Y.; Bushard, P. J.; Weiss, E. A.; Wasielewski, M. R. *J. Am. Chem. Soc.* **2002**, *124*, 9582. (c) Fuller, M. J.; Sinks, L. E.; Rybtchinski, B.; Giaimo, J. M.; Li, X.; Wasielewski, M. R. *J. Phys. Chem. A* **2005**, *109*, 970.

(4) (a) Wang, Z.; Medforth, C. J.; Shelnutt, J. A. *J. Am. Chem. Soc.* **2004**, *126*, 15954. (b) Schwab, A. D.; Smith, D. E.; Rich, C. S.; Young, E. R.; Smith, W. F.; de Paula, J. C. *J. Phys. Chem. B* **2003**, *107*, 11339. (c) Sostaric, J. Z.; Pandian, R. P.; Weavers, L. K.; Kuppusamy, P. *Chem. Mater.* **2006**, *18*, 4183. (d) Kojima, T.; Harada, R.; Nakanishi, T.; Kaneko, K.; Fukuzumi, S. *Chem. Mater.* **2007**, *19*, 51. (e) Karthaus, O.; Nagata, S.; Nishide, J.; Sasabe, H. *Jpn. J. Appl. Phys.* **2008**, *47*, 1245. (f) Zhang, X.; Sun, B. *J. Phys. Chem. B* **2007**, *111*, 10881. (g) Yan, P.; Chowdhury, A.; Holman, M. W.; Adams, D. M. *J. Phys. Chem. B* **2005**, *109*, 724. (h) Su, W.; Zhang, Y.; Zhao, C.; Li, X.; Jiang, J. *ChemPhysChem* **2007**, *8*, 1857. (i) Brisbeno, A. L.; Mannsfeld, S. C. B.; Reese, C.; Hancock, J. M.; Xiong, Y.; Jenekhe, S. A.; Bao, Z.; Xia, Y. *Nano Lett.* **2007**, *7*, 2847.

(5) (a) Zhao, L.; Yang, W.; Ma, Y.; Yao, Y.; Lib, Y.; Liub, H. *Chem. Commun.* **2003**, 2442. (b) Bai, R.; Ouyang, M.; Zhou, R.-J.; Shi, M.-M.; Wang, M. H.-Z. *Nanotechnology* **2008**, *19*, 055604. (c) Kriha, O.; Goring, P.; Milbradt, M.; Agarwal, S.; Steinhart, M.; Wehrspohn, R.; Wendorff, J. H.; Greiner, A. *Chem. Mater.* **2008**, *20*, 1076. (d) Cho, S. I.; Lee, S. B. *Acc. Chem. Res.* **2008**, *41*, 699.

(6) (a) Tang, Q.; Li, H.; Liu, Y.; Hu, W. *J. Am. Chem. Soc.* **2006**, *128*, 14634. (b) Rakow, A. N.; Suslick, K. S. *Nature* **2000**, *17*, 710. (c) Tang, Q.; Li, H.; Song, Y.; Hu, W.; Jiang, L.; Liu, Y.; Wang, X.; Zhu, D. *Adv. Mater.* **2006**, *18*, 3010. (d) Tong, W. Y.; Djurisic, A. B.; Xie, M. H.; Ng, A. M. C.; Cheung, K. Y.; Chan, W. K.; Leung, Y. H.; Lin, H. W.; Gwo, S. *J. Phys. Chem. B* **2006**, *110*, 17406. (e) Xiao, K.; Tao, J.; Pan, Z.; Puretzky, A. A.; Ivanov, I. N.; Pennycook, S. J.; Geohegan, D. B. *Angew. Chem.* **2007**, *119*, 2704. (f) Fan, Z. Y.; Mo, X. L.; Chen, G. R.; Lu, G. L. *Rev. Adv. Mater. Sci.* **2003**, *5*, 72. (g) Mbenkum, B. N.; Barrena, E.; Zhang, X.; Kelsch, M.; Dosch, H. *Nano Lett.* **2006**, *12*, 2852. (h) Barrena, E.; Zhang, X. N.; Mbenkum, B. N.; Lohmueller, T.; Krauss, T. N.; Kelsh, M.; Van Aken, P. A.; Spatz, J. P.; Dosh, H. *ChemPhysChem* **2008**, *9*, 1114. (i) Borras, A.; Aguirre, M.; Groening, O.; Lopez-Cartes, C.; Groening, P. *Chem. Mater.* **2008**, *20*, 7371. (j) Borras, A.; Groening, O.; Juergen, K.; Groening, P. *Adv. Mater.* **2009**, *21*, 4816. (k) Borras, A.; Groening, P.; Sanchez-Valencia, J. R.; Barranco, A.; Espinos, J. P.; Gonzalez-Elipe, A. R. *Langmuir* **2010**, *26*, 1487. (l) Ng, A. M.-C.; Djurisic, A. B.; Tam, K.-H.; Kwok, W.-M.; Chan, W.-K.; Tam, W. Y.; Phillips, D. L.; Cheah, K.-W. *Adv. Funct. Mater.* **2008**, *18*, 566.

phase of the nanofibers or to produce high-density arrays and patterned structures. On the other hand, the template method, although being a very powerful tool, presents as limitation that the elimination of the template material hampers its applicability at large scales. Therefore, the vapor transport methods stem as one of the most straightforward routes for organic nanofibers and nanotubes fabrication. However, most of the examples in the literature regard the deposition of metallophthalocyanine nanofibers and the growth of perylene nanofibers growth is almost unexplored.[6j] Metallophthalocyanine nanofibers have been successfully prepared by solid vapor growth following different methodologies.[6] Xiao et al.[6e] have reported the formation of copper−tetracyanoquinodimethane (Cu-TCNQ) nanofibers by deposition of TCNQ on a Cu thin film. By this process, the TCNQ vapor reacts chemically with the Cu surface, leading to the formation of single-crystal conical nanofibers. In a similar way, Ag-TCNQ nanofibers were produced by reaction of the TCQN with a silver layer.[6f] Barrena et al.[6g,h] have shown the growth of F16CuPc nanotubes and nanofibers on gold particles by a base-growth mechanism. A metal-free route based on the use of indium tin oxide (ITO) and silicon substrates with thermal activation has been studied by Tang et al.[6a] However, none of the previous methodologies permitted the controlled growth of organic nanofibers on both metallic and nonmetallic substrates. Very recently, we have published the basis of a physical vapor deposition (PVD) method for the production of both metalloporphyrin and metallophthalocyanines nanofibers on heterocomposite silver/Si(100) substrates.[6i] In the case of the perylene-related compounds, its fabrication in the form of 1D nanostructures has been recently reported in different works via several deposition methods.[4e−i,6] In this context, the development of a universal method for the growth π-conjugated molecules in form of crystalline supported nanofibers would be of the utmost interest and significance.[1] Thus, the main objective of the present work is to report the generalization of our methodology[6i] to the production of supported single-crystalline nanowires with π-conjugated molecules. Two aspects are specifically addressed: First, extending the applicability of the method for any kind of nanowire composition: MePTCDI, metalloporphyrin, and metallophthalocyanine. Second, we study the impact of the type of substrate on the development of the nanowires. Herewith, we compare the effect of flat substrates coated by a thin silver layer[6i,7a,8] and of nonmetallic surfaces such as TiO_2, ZnO, SiO_2, and Ta_2O_5 thin films.[7b−d] Several factors are proposed as determinant in the nanowires growth: substrate roughness and temperature, growth rate and deposition time, among others. A thorough investigation by TEM of the single-crystalline nanowires has permitted us to elucidate the arrangement and stacking mode of the molecules along the nanowires. Based on the results of this investigation, a growth mechanism of the nanowires is proposed. In addition, the application of the ideas of this model has allowed the synthesis of two particular families of semiconductor nanowires: "binary nanofibers" formed by two miscible molecules and "open core@shell nanofibers" obtained by the sequential growth of two different types of nanofibers on the same substrate.

Scheme 1. Chemical Structures of M-OEP, M-Pc, and Me-PTCDI, As Labeled

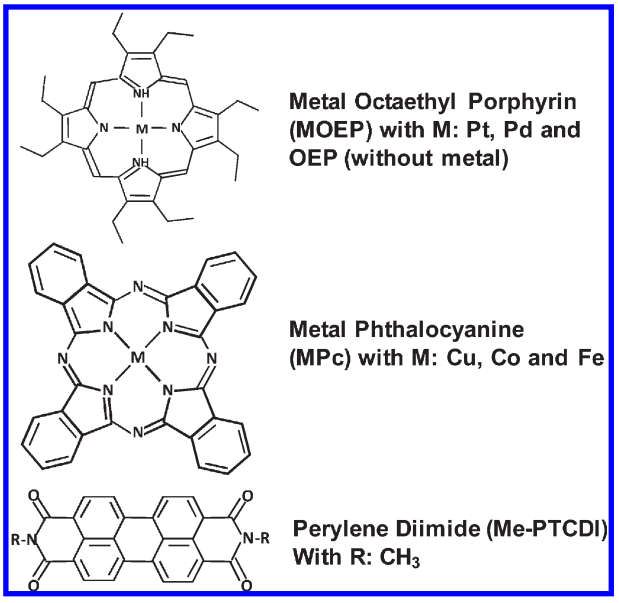

Experimental Section

Perylene diimide (2,9-dimethylanthra[2,1-*def*:6,5,10-*d*′*e*′*f*′]diisoquinoline-1,3,8,10-tetrone (Me-PTCDI) from Sensient Imaging Technologies), porphyrins (Frontier Scientific), and phthalocyanines (Aldrich) were used as purchased (see Scheme 1 for their molecular structures). The sublimation of the molecules for the nanowires deposition was carried out in a 10 cm^3 OLED Knudsen cell (Lesker) placed in a high-vacuum chamber. A second hand-made evaporation cell was located at the same plane for the growth of the heterostructured nanowires. The system was pumped up to 5×10^{-6} mbar base pressure before the deposition. The distance between the substrate and the sublimation source was 8 cm. During the experiments argon was dosed using a calibrated mass flow controller (MKS). The pressure in the system during deposition was fixed at 0.020 mbar. The growth rate was controlled by a quartz crystal microbalance located in the same plane as the substrates. The deposition rates were between 0.30 and 0.50 Å s^{-1} considering a density in the balance of 0.5 g cm^{-3}. An estimated time of 20−30 min was necessary for the wires formation. A schematic of the deposition system is shown in the Scheme S1 in the Supporting Information. Further information can be founded elsewhere.[7g] For the Me-PTCDI the optima temperature was 175 ± 5 °C; for the porphyrins, the temperatures varied between 140 ± 5 °C, for OEP and PtOEP, and 150 ± 5 °C, for the PdOEP. A higher value of 220 ± 5 °C was necessary for the growth of CuPc nanowires and about 240 ± 5 and 260 ± 5 °C for the FePc and CoPc, respectively. From now on we will designate with $T_{substrate}$ the temperature measured of the substrate during the deposition and with T_{Cell} the temperature of sublimation of the molecules. We understand T_{Cell} as the temperature measured by a thermocouple inserted in the 10 cm^3 OLED Knudsen cell in the preparation chamber at 0.020 mbar of Ar when the thickness measurement in the QMC emplaced at the same level of the substrate holder is stable about 0.1 Å s^{-1}.

Different substrates were coated simultaneously during the experiments. Si (100) wafers, copper grids, quartz, and borosilicate glass slides (Corning) were used as reference substrates.

In this article we follow to demonstrate that the growth of organic nanowires is mainly dependent on the substrate morphology and roughness; i.e., its metallic or nonmetallic nature does not affect the nanostructures development. With this aim, several

(7) (a) Borras, A.; Barranco, A.; Espinos, J. P.; Cotrino, J.; Holgado, J. P.; Gonzalez-Elipe, A. R. *Plasma Process. Polym.* **2007**, *4*, 515. (b) Borras, A.; Yanguas-Gil, A.; Barranco, A.; Cotrino, J.; Gonzalez-Elipe, A. R. *Phys. Rev. B* **2007**, *76*, 235303. (c) Borras, A.; Sanchez-Valencia, J. R.; Garrido, J.; Barranco, A.; Gonzalez-Elipe, A. R. *Microporous Mesoporous Mater.* **2009**, *118*, 314. (d) Martín, A.; Espinos, J. P.; Justo, A.; Holgado, J. P.; Yubero, F.; Gonzalez-Elipe, A. R. *Surf. Coat. Technol.* **2002**, *151−152*, 289. (e) Sanchez-Valencia, J. R.; Borras, A.; Barranco, A.; Rico, V. J.; Espinos, J. P.; Gonzalez-Elipe, A. R. *Langmuir* **2008**, *24*, 9460. (f) Rico, V.; Borras, A.; Yubero, F.; Espinos, J. P.; Frutos, F.; Gonzalez-Elipe, A. R. *J. Phys. Chem. C* **2009**, *113*, 3775. (g) Barranco, A.; Groening, P. *Langmuir* **2006**, *22*, 6719.

(8) Fergus, J. W.; Mallipedi, C. V. S.; Edwards, D. L. *Composites, Part B* **1998**, *29B*, 51.

types of substrates were included in every experiment: silver and gold thin films, columnar and flat TiO_2 thin films showing different microstructures and surface roughness prepared by plasma enhanced chemical vapor deposition (PECVD);[7b,c] ZnO columnar thin films deposited by PECVD,[7d] columnar Ta_2O_5 and columnar SiO_2 thin films deposited by gracing angle physical vapor deposition (GAPVD),[7e,f] and ultraflat layers of SiO_2 obtained by plasma oxidation of a Si wafer. Both silver and gold substrates were deposited by a simple dc sputtering method at room temperature.[7a] The density, i.e., number of nanowires, increases when the metal substrates are oxidized by plasma. The oxidation pretreatment was carried out in situ by placing a microwave electron cyclotron resonance (MW-ECR) reactor working in a remote configuration (see Scheme S1 and refs [6i] and [7g]). The amount of silver required for an optimal deposition of the nanofibers was measured before the plasma treatment by SEM: Ag(1) < 15 nm for the Me-PTCDI, Ag(2) ~ 30 nm for the porphyrins, and Ag(3) ~ 60 nm for the phthalocyanines. The label Ag(4) refers to silver in bulk.

For transmission electron microscopy (TEM) analysis the nanowires were grown on copper grids previously covered with silver. Two different transmission microscopes were used for a full characterization of the nanowires. The high-resolution images were acquired in a CM 300 from Phillips. The crystalline structured of the samples was studied by selected area electron diffraction (SAED) on a Tecnai F30 TEM operating at an acceleration voltage of 300 kV and equipped with Schottky field emission electron source and Super Twin lens. High-resolution SEM images were obtained in a Hitachi S4800 and in a Hitachi S5200 at different acceleration voltage (1−5 kV). The UV−vis transmission spectra of samples deposited on glass slides were recorded in a Cary 50 spectrophotometer in the range from 200 to 1100 nm.

Results and Discussion

Generalization of Methodology for Perylene, Porphyrins, and Phthalocyanines. By vacuum deposition of the molecule species on silver/Si(100)[6i] at controlled growth rate and temperature of the substrate, we have successfully synthesized different 1D nanostructures including perylene diimide (Me-PTCDI), octaethylporphyrin (OEP), platinum and palladium octaethylporphyrins (PtOEP and PdOEP), and copper, iron, and cobalt phthalocyanine (CuPc, FePc, and CoPC) nanowires. The chemical structures of these molecules are shown in Scheme 1.

Our investigations have shown that the nanowire growth is a temperature-activated process in all the studied systems. The ideal temperature of the substrates ($T_{substrates}$) is different for each type of molecule, and it is directly related with its sublimation temperature (T_{Cell}).[6i] As we will demonstrate in this work, the formation of high aspect ratio nanowires is achieved whenever the temperature of the substrates ($T_{substrates}$) and the sublimation temperature of the organic molecule in Ar atmosphere (T_{Cell}) satisfy the condition $T_{substrates} > 0.7T_{Cell}$ for the porphyrins and phthalocyanines and $T_{subs} > 0.6T_{Cell}$ for the perylenes. In addition to the pronounced temperature dependence it has been realized that the thickness of the silver layer on the substrate is also a key parameter for the control of the growth of the organic nanostructures and its value has to be adjusted for each system. Generally, we observe that the fabrication of phthalocyanine nanowires requires a thicker layer of silver around ~60 nm (Ag(3)), while the porphyrin nanowires grow on ~30 nm (Ag(2)) and the Me-PTCDI nanofibers on ~15 nm (Ag(1)). Out of these studies it is found that the grainlike morphology of the silver/Si (100) substrates is actually the main property controlling the nanowires growth. As is shown below, the grainlike morphology of the heterosubstrates Ag/Si or Ag/quartz is produced by the silver nanoparticle formation on flat substrates either after heating treatment of the substrates at the different $T_{substrates}$ or by plasma oxidation. In such a manner that the requirements about the optimal silver thickness for the NWs growth are translated to requisites about the size distribution of the particles formed in the substrates and therefore to the surface roughness of the substrates.

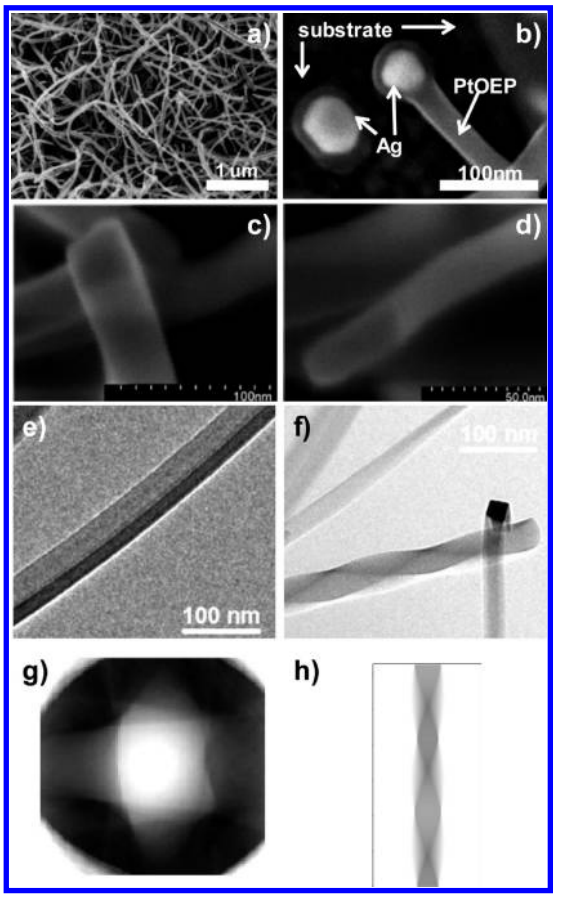

Figure 1. (a) Planar view SEM micrograph of the surface containing a high density of Me-PTCDI nanowires. (b) High-resolution SEM image of a PtOEP nanowire growing from the silver particle. (c, d) High-resolution SEM images of Me-PTCDI nanowires. (e, f) TEM micrographs of a belt-shaped Me-PTCDI nanowires and a twisted CuPc nanowires, respectively. (g) Reconstructed cross section of the twisted nanowire in (f) obtained by a tomographic analysis. (h) TEM image simulation of a nanowire with cross section of 1.25 after twisted along its axis.

Morphological and Structural Analysis of the Organic Nanowires. Figure 1a shows a planar view SEM micrograph of the Me-PTCDI nanowires deposited on a silver/Si(100) substrates with thickness ~15 nm, i.e. substrate Ag(1), at 175 °C. A thorough analysis of the wires by HRSEM and TEM reveals that the nanowires grow from the particle at its base following a rectangular shaped footprint with a largely invariant cross section over their whole length and a smooth surface (Figure 1b−d).

When the deposition process is carried out at normal conditions, nanowires with different aspect ratio of their footprint are formed. Figure 1d,e shows different Me-PTCDI rectangular nanobelts and Figure 1c a squared Me-PTCDI nanofiber. The widths of the flat nanofibers or nanobelts are in the range from 20 to 150 nm, with aspect ratios as high as 4. For the squared nanofibers, the widths vary between 20 and 75 nm (cf. Figure S1 in Supporting Information). The thickness distribution histograms gathered in Figure S1 stress the similarities of the width distributions of the nanowires formed by the different molecules under

study. These results further confirms that nanowires formed by different molecules present similar morphologies corresponding either to squared nanofibers or nanobelts. Moreover, the slight differences in the histograms in Figure S1 might be related to the different sizes and geometry of the molecules forming the nanowires and the sticking coefficient of the molecules on the substrates among other factors. For the M-Pc and M-OEP nanofibers, lengths from 0.2 to 5 μm can be obtained by varying the deposition time. However, under similar deposition conditions perylene nanowires as long as 30 μm were obtained (see Figure S2). These squared nanofibers and nanobelts are characterized by a high flexibility and facility to bend and twist.[6d,i] The CuPc squared nanofiber in the TEM micrograph in Figure 1f depicts one of the possible movements of these structures, consisting of a twist around the longitudinal axis of the fiber. To show that this structure was originally a squared nanofiber, we carried out a tomographic reconstruction of the TEM image. Effectively, the resulting cross section along the nanofiber axis in Figure 1g is in agreement with this hypothesis. Moreover, the TEM image simulation of an almost squared nanofiber (rectangular cross section with a/b = 1.25) after it is completely twisted along its length also supports this assumption (Figure 1h). The origin of the formation of such twisting or helical fiber is presumably an anisotropic surface stress.[9a] In fact, during the characterization of the nanofibers by SEM and TEM, we could observe the formation of the twisted nanowires under the electron beam.

The structural characterization of the nanowires was carried out by TEM, high-resolution transmission electron microscopy (HRTEM), and selected area electron diffraction (SAED). A theoretical study of the structure of the nanowires is presented in the Supporting Information. The different possible arrangements of the molecules following a π-stacking along the nanowire axis and their corresponding predicted SAED patterns are depicted in Figure 2 and Figures S3−S7. It is worth to remark that this kind of material suffers a fast amorphization under the electron beam that hinders its full characterization by TEM. Indeed, the examples in the literature usually report on thicker fibers when the SAED patterns are presented. By contrast, the results of the structural analysis summarized in Figure S8 were acquired for different nanowires with thickness in the range between ~20 and 70 nm. Along with the amorphization by the beam, the sharp and bright spotted patterns characteristics of a single-crystalline nanofiber (Figure S8a,d) turn into diffuse rings (Figure S8b). The SAED patterns from a CoPc nanofiber before and after a few seconds of exposure to the beam show clearly these changes (Figure S8a,b).

As a conclusion from the SAED studies, we can affirm that independently of the molecular composition all the nanowires are single crystals. By comparison with the ED simulated in Figure 2 and in the Supporting Information, the arrangement of the molecules along the wire results in a columnar structure where the molecules are forming a herringbone stacking. Such a structure is produced by the molecules forming columns along the wire axis via strong $\pi-\pi$ interactions and exhibiting an angle with respect to the columns axis. This tilt angle is close to 15° for the porphyrins and phthalocyanines and to 30° for the perylenes. It is expected that van der Waals interaction acts between molecules in neighboring columns. A random, uncorrelated offset of the columns in the wire direction (z-direction) causes that some of the spots in the SAED pattern appear diffuse. Moreover, the

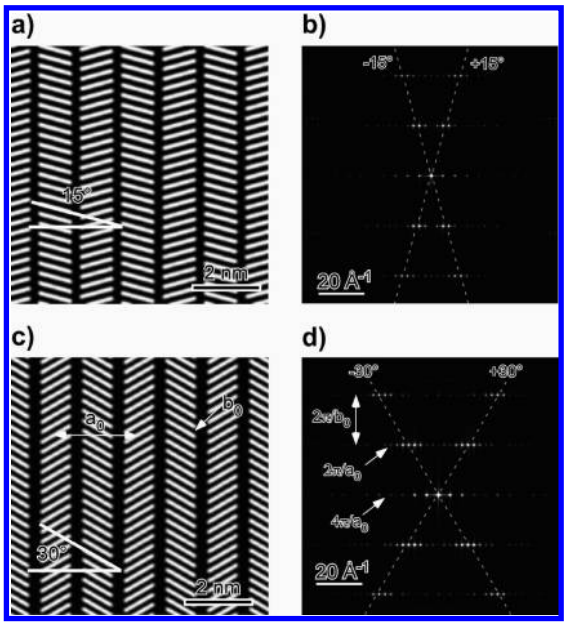

Figure 2. Columnar stacking of the molecules with a periodicity of b_0 = 0.29 nm along the columns. The columns are stack in a herringbone fashion with a periodicity of a_0 = 2.44 nm. The position of the columns is correlated, which means that there is no random offset between the columns. In (a) the real space intensity map is shown for a tilt angle of 15° and in (c) for 30°. (b) and (d) show the corresponding Fourier transforms. In the diffraction the tilt angle is expressed in the vertical tilt angle of the diffraction spots. The line spacing in the vertical direction corresponds to $2\pi/b_0$. The spots spacing on a line is different for the zero order spot (spacing equals to $4\pi/a_0$, which means a real space spacing of $a_0/2$) and the high-order lines which show the usual $2\pi/a_0$ spot spacing.

HRTEM image of a CoPc nanobelt in Figure 3a is also compatible with this columnar formation. The well-defined striped structure along the nanowire axis is formed by 17 columns of an approximate width of 1.23 nm. This value is comparable with the diameter of the CoPc molecule, and therefore it is in good agreement with a herringbone stacking, i.e., tilt angle ~15°, of the molecules forming the different columns. The HRTEM image of a twisted squared CoPc nanofiber in Figure 3b shows a similar result. Thus, both kinds of nanowires can be described by a columnar structure of molecules following a herringbone stacking. As far as we know, this is the first time that such a clear stacking is demonstrated by HRTEM for an organic nanofiber.

Generalization of the Methodology for Metallic and Nonmetallic Substrates. After the full characterization of the nanofibers morphology and structure, the role played by the silver layer in the process and the origin of the formation of squared nanofibers and nanobelts remain to be elucidated. As a matter of fact, other metallic substrates made of gold layers were successfully used to grow nanowires (cf. Figures S9 and S10 in the Supporting Information). In these studies, different kinds of nanobelts and squared nanofibers grew on the gold substrate, being the type of structures mostly dependent on the morphology of the gold substrate. The growth on gold thin films resulted in the formation of large nanobelts showing a lamellar microstructure (Figure S9); meanwhile, on substrates decorated with gold nanoparticles the nanowires development into nanobelts or squared nanofibers was similar to those on silver nanoparticles (Figure S10). The strong dependence of the nanowires morphology on the roughness has been pointed out already in the case of the silver substrates in our previous work,[6i] and it will be discussed

(9) (a) Wang, J. S.; Feng, X. Q.; Wang, G. F.; Yu, S. W. *Appl. Phys. Lett.* **2008**, *92*, 191901. (b) The crystal shown is a combination of cube−octahedrons−dodecahedron with symmetry 4/m3bar2/m. Erk, P.; Hetzenegger, J.; Böhm, A. *Eur. Coat. J.* **1997**, 906.

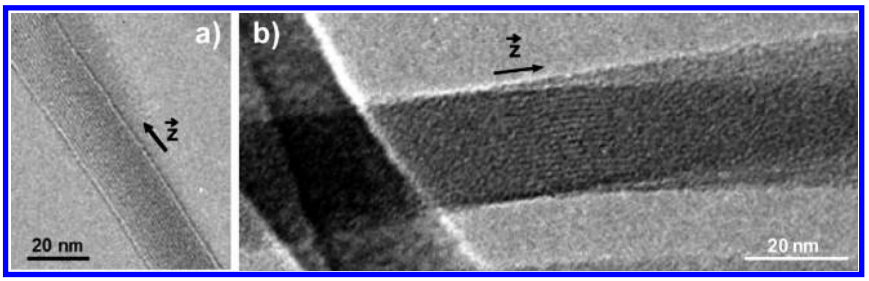

Figure 3. HRTEM micrographs of a CoPc nanobelt (a) and a twisted CoPc squared nanofiber (b).

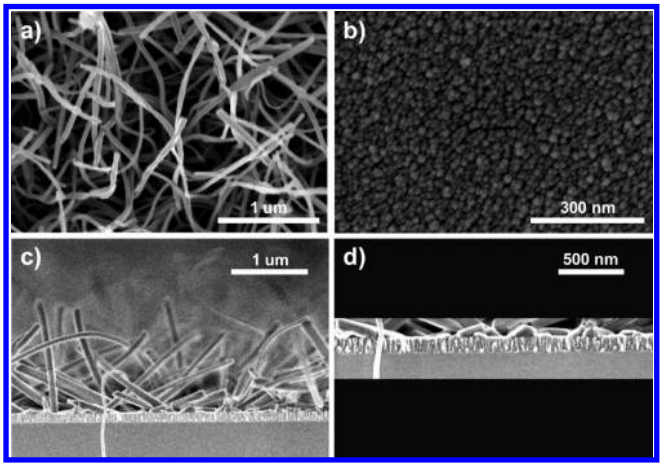

Figure 4. Growth of organic nanowires on TiO_2. (a) Planar view SEM micrograph of the Me-PTCDI nanowires deposited on the surface of a TiO_2 thin film. (b) The corresponding SEM image of the TiO_2 surface. (c, d) Cross-section SEM micrographs of the Me-PTCDI nanowires growing from the TiO_2 thin film. The columnar microstructure of the TiO_2 is clearly visible in (d).

in detail in the following section. Substrates of controlled microstructure and roughness and nonmetallic surface were included in the experiments with the aim of elucidating whether the metallic character of the substrate was a essential requirement.[7] Figure 4 shows the growth of Me-PTCDI on a columnar and porous TiO_2 substrate at 175 °C ($\sim 0.6T_{Cell}$) (see the optical properties of these samples in Figure S11). The morphological study of the nanowires on TiO_2 reveals that the growth on this substrate is completely analogous to the growth on Ag(1) (cf. Figure 1a). The most plausible reason for this is that such substrates present similar features sizes at different scales. The structures contributing to the roughness on the largest scale are features of roughly 50 nm diameter or larger depending of the film thickness, which are formed by the columnar microstructure (Figure 4b,d). The roughness on a second, smaller length scale (features ~5 nm) is due to the intrinsic roughness of each column.[7b] These scales match with the variations in the particles distribution observed for the silver substrates (Ag(1) to Ag(3)). The formation of squared nanofibers and nanobelts occurs in a similar way for both the TiO_2 and the silver and gold nanoparticulated substrates. The experiments summarized in Figures S12−S15 in the Supporting Information further demonstrate that the columnar microstructures of other oxide thin films deposited by various techniques (ZnO, SiO_2, and Ta_2O_5) also provide suitable surfaces regarding the growth of Me-PTCDI, M-Pc, and M-OEP nanofibers. Therefore, we can conclude that the growth of the organic nanowires is independent of the chemical composition of the substrate.

Factors Controlling the Growth of Organic Nanowires by Physical Vapor Deposition. Growth Mechanism. Our results address that the growth mechanism responsible for the nanowires

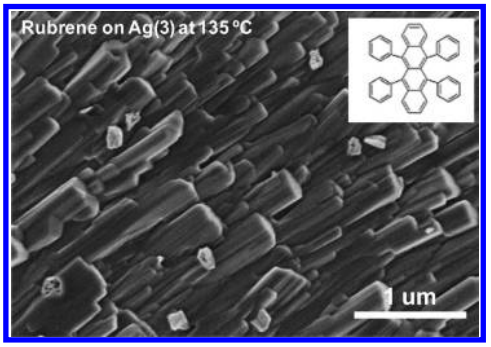

Figure 5. SEM image of the surface of a rubrene thin film formed on the Ag(3) substrate at 135 °C.

formation is a crystallization process driven by the strongly directionality of the π-stacking. As a crystallization process from a homogeneous phase (vapor), it must be dominated by a supersaturation regime. The level of supersaturation depends among other factors on the number of molecules impinging the substrates, the temperature of the substrates, and the possible defects or impurities that can act as nucleation sites for the crystal. These three factors are exactly the variables that we try to control in the methodology of our synthesis. We have carried out an in deep study from a phenomenological point of view of the nanowires formation. In this section we present the experiments that have permitted us to point out the main factors involved in the formation of a high density of supported organic nanowires and to elucidate the growth mechanism.

a. Comparison with Herringbone-Packing Organic Molecules. In this article we report on the generalization of the methodology for metalloporphyrins, metallophthalocyanines, and perylene molecules. All these molecules present face to face stacking (π-stacking). This stacking is common in molecules that possess a two-dimensional extended aromatic system. Different experiments with molecules forming other type of stacking were carried out in order to demonstrate that the self-assembly of the molecules by π-stacking is a *sine qua non* requirement in the formation of the nanowires. As an example, Figure 5 shows a polycrystalline thin film formation resulting of the growth of rubrene, a molecule displaying a herringbone-stacking instead of face to face stacking. No nanowires growth was observed for rubrene on different substrates in any experimental conditions.

b. Dependence on the Deposition Growth Rate. One of the ways to achieve the supersaturation of the medium is to increase the number of molecules reaching the surface. Because of the nature of our methodology, a physical vapor deposition at low and constant pressure, this condition can be translated to the variation of the growth rate measured in the QCM. Figure S16 shows the deposition at different growth rate of CuPc for the same substrate and substrate temperature. The first important result extracted from this figure is the no formation of nanowires for low

growth rates (Figure S16a); i.e., there is a lower limit in the growth rate to produce the nanowires. Above this limit a high density of nanowires is formed on the surface (Figure S16b). For higher values of the growth rate the nanowires formed are generally thicker (Figure S16c).

c. Roughness and Morphology of the Substrates. Evidence for the Nucleation Sites. A fundamental factor in the process of crystallization on a surface is the presence of nucleation sites. We follow to demonstrate that the role played by the metallic particles and the oxide grains is exactly to provide the nucleation sites for the formation of the single crystal nanofibers. Figure S17 gathers the comparison between the PtOPE nanowires development on a Ag(2) thin film (left) and a Ag(2) thin film after the in situ oxidation treatment by plasma (right). Both experiments were carried out at 140 °C; thus, the compact silver thin film microstructure is modified (see also Figure S18). These experiments altogether with those in Figures S9 and S10, regarding gold thin films and gold nanoparticles, show that the density and homogeneity of the nanowires on the silver and gold thin film previous to the plasma treatment were very low. As we have demonstrated in a previous article (see ref [7a]), due to the plasma treatment the thin film morphology changes from a homogeneous thin film to a heterostructured substrate where the free space between the metal particle is easily visible by SEM (see Figure S18). On other hand, the silver oxide is reduced in Ar atmosphere at temperatures higher than 160 °C; in the case of NPs this temperature is expected to be lower.[8] Thus, at the normal conditions of the growth of the nanowires the silver is metallic in both pretreated and nonpretreated substrates. Consequently, it seems that the differences in the formation of the nanowires between the substrate in Figure S17 (left and right) are originated by the differences in the silver particles grain morphology and particle sizes distribution. Moreover, we have already indicated that the formation of a high density of nanowires depends on the thickness of the silver layer and on the type of molecule. Figure S19 shows the deposition under the same experimental conditions of PtOEP on a Si(100) wafer (a), silver substrates of several thicknesses (b−d), and on amorphous TiO_2 thin films with flat (e) and columnar (f) microstructures. The approximated rms values for the silver substrates after the plasma treatment were measured by AFM for 1 μm × 1 μm areas: Ag(1) < 5 nm; Ag(2) ~ 8−15 nm, and Ag(4) > 15 nm. The TiO_2 thin films utilized in this study were deposited by PECVD at room temperature.[7b] Depending on the experimental conditions both columnar and homogeneous TiO_2 thin films can be deposited. The surface roughness of the TiO_2 depends on the microstructure and thickness of the thin film.[7b] The rms values for the columnar TiO_2 films are in the range between 2 and 10 nm and for the flat TiO_2 below 1 nm.[7b] On flat substrates (Figure S19a,e) without nucleation sites very few nanowires appear, being shorter and thicker than those in the silver substrates and columnar TiO_2. In fact, the result of the PtOEP deposition at 140 °C on the Si(100) is rather a compact film. The nanowires density and homogeneity increase as the silver thickness (Figure S19b,c). However, for higher amount of silver, Ag(3) and Ag(4), i.e., for a higher amount of silver particles and roughness of the surface, the number or PtOEP nanowires falls drastically. However, it is important to note that although the limits of the surface roughness for the optimal formation of the NWs depend on the type of molecules for molecules of the same family with different metal cations (e.g., CoPc and FePc or PtOEP and PdOEP) the requirements about the surface roughness are similar. In the case of the TiO_2 substrate the different surface topography also affect clearly to the formation of the nanowires. Almost no nanowires of PtOEP grow on the flat TiO_2; meanwhile, a very high density of PtOEP nanowires

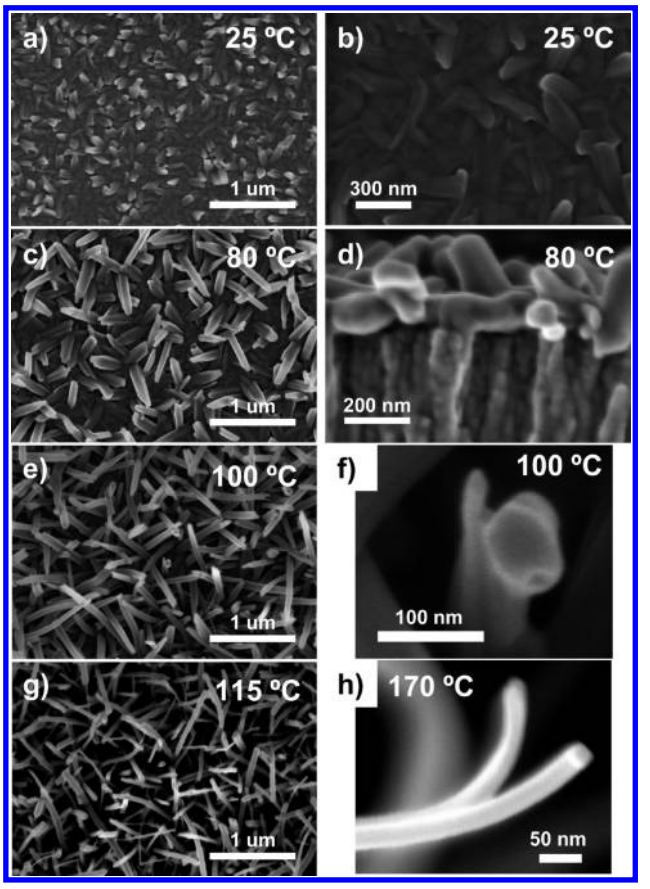

Figure 6. Normal view SEM (a−c, e−g) and cross-section images of the deposition of PtOEP on columnar TiO_2 substrates at different $T_{substrates}$ as labeled. (h) High-resolution SEM image of squared nanofibers grown at 170 °C.

are formed on the columnar TiO_2 (cf. Figure S19e,f). In summary we have demonstrated that the formation of a high density of ONWs is directly related to the number and size of the features on the substrate. These features or motifs acting as nucleation sites and basis of the nanowire growth can be a metal particle, an oxide grain, or any defect within a range of sizes and distributions.

d. Microstructure Evolution with the Substrate Temperature. The study of the sublimation of the π-conjugated molecules at different temperature of the substrates has revealed that the nanowire growth is a temperature-activated process in all the studied systems. Figure S19c shows a high density of PtOEP nanofibers grown at 140 °C; however, for the same $T_{substrates}$ the deposition of CuPc (Figure S20a) results in the formation of rodlike grains and very few and irregular fibers. For higher $T_{substrates}$ (Figure S20b) the growth of CuPc produces nanowires similar to those in Figure S19c. Indeed, the ideal temperature of the substrates to achieve a high density of squared NFs and nanobelts depends on the organic molecule, and it is directly related with its sublimation temperature (T_{Cell}).[6i] For the standard experimental setup and conditions listed in the Experimental Section, the formation of a high density of nanowires is achieved for the following T_{Cell} to $T_{substrates}$ relations: $T_{substrates} > 0.7T_{Cell}$ for the porphyrins and phthalocyanines and $T_{substrates} > 0.6T_{Cell}$ for the perylenes. The existence of a critical temperature for the nanowires formation depending on the sublimation temperature is in very good agreement with a crystallization mechanism given that within this process it is very important that the balance between the adsorption and desorption of the molecules at the substrate level.

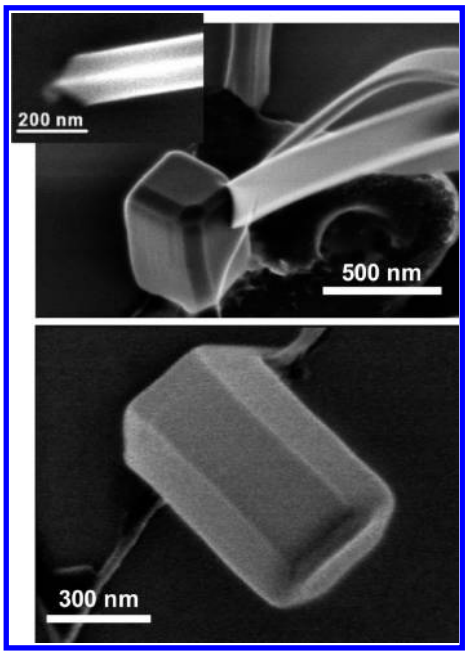

Figure 7. SEM images showing some details of Me-PTCDI nanostructures grown on SiO_2.

On other side, we carried out a thorough study of the deposition of the organic molecules at very different substrate temperatures in order to fully understand the relationship among the critical temperature and the sublimation temperature of the molecules. Figure 6 shows the deposition of PtOEP on columnar TiO_2 at different T_{sust}, from RT to 170 °C, i.e., for $T_{substrates} \sim 0.125T_{Cell}$ to $T_{substrates} \sim 0.85T_{Cell}$ (see also Figure S19f). Since the microstructure of the TiO_2 thin film does not change in this range of temperatures, we can ensure that the changes in the PtOEP microstructure are not induced by variations of the substrate morphology.

At low $T_{substrates}$ the deposition of the organic molecules produces a thin film of high compactness and roughness (Figure 6a,b). As the $T_{substrates}$ increases, the thin film thickness decreases and its surface is dominated by the presence of short 1D structures (Figure 6c,d). For $T_{substrates}$ closer to $0.5T_{Cell}$ no thin film formation remains, and the layer is formed for a high density of hexagonal-shaped nanofibers (Figure 6e,f). These nanorods spark off to the squared nanofibers and nanobelts for slightly higher temperatures of the substrates (Figure 6g), seeing visible some hexagonal rods yet. For $T_{substrates} \sim 0.7T_{Cell}$ only squared nanofibers and nanobelts, i.e., rectangular shaped nanofibers, are formed. For higher $T_{substrates}$ the nanowires are longer and thinner but in a lower number, being more numerous the squared nanofibers than the nanobelts (Figure 6h and ref [6i]).

e. Formation of Crystals Following Different Crystal Habits. Figure 7 shows the growth of Me-PTCDI on flat and compact SiO_2 at 265° ($\sim 0.9T_{Cell}$). In our previous work[6i] and subsection d we have shown that for the organic nanowires on Ag/Si(100) and columnar oxide substrates the increase in the $T_{substrates}$ provokes the preferential formation of the squared nanofibers that, in this case, are thinner and longer. However, the growth of Me-PTCDI on flat SiO_2 at high $T_{subtrates}$ presents different characteristics. In the case of the Me-PTCD, the sticking coefficient of the compound on the flat SiO_2 is very low, and just a few nanowires appear on the defects of the substrate. Along with the squared nanofibers and nanobelts (Figure 7, top and top, inset), other Me-PTCDI crystalline aggregates can be found in these samples.

The forms of the faceted crystals in Figure 7 are characteristic of the permitted crystal habits of the perylene diimide. For instance, the central feature in Figure 7 (top) corresponds to the isomeric system.[9b] This characteristic form is a consequence of a crystal growth dominated by a fast development following one of the possible crystalline directions (in this case, the (011)).[9b]

f. Dependence on the Deposition Time. In order to fully understand the development of the nanowires, we have studied the deposition of the PtOEP under the more favorable conditions for different deposition times measured by the thickness in the QCM (Figure S21). First of all, at the sight of the results in Figure S21 it is clear that the amount of nanowires increases with the deposition time. In such a way that for very short times only part of the particles on the substrate are acting as nucleation site (Figure S21a). For longer deposition times, the density of nanowires increases and also the length of the nanowires already formed (Figure S21b). Eventually, almost all of the nucleation sites are covered, and the nanowires continue growing in length (Figure S21c). It is worthy to stress that the formation of the NWs is a very fast process, in agreement with a crystal formation. Interestingly, once the nanowire is formed, the most important change is in length; meanwhile, the thickness increment is very slight. Furthermore, the shape of the nanowire is already determined at the first stages of its formation. This latter result indicates that the morphology of the nanowires can be consequence either related with the different growth rates according to the crystal directions or by the fusion of various squared fiber nuclei growing from nearby nucleation sites providing a belt. In fact, the growth under certain conditions of lamellar structures such the CuPc nanofibers on Figure S9b could support the latter hypothesis. However, the formation of squared nanofibers and nanobelts via solution methods[1b,4] without any influence of external nuclei compelled us to keep this question open.

After the full analysis of the samples by different techniques (HRTEM, SEM, and EDX) where no trace of silver was found along or on the top of the nanowires, the vapor−liquid−solid mechanism (VLS) and the chemical reaction with the silver on the substrate are rejected as growth mechanisms. On the other hand, the phenomenological study on the factors controlling the nanowires growth indicates that their formation implies a crystallization process. Under certain conditions, this process leads to the development of crystals in form of nanobelts and squared nanofibers.

The growth and development of the crystal follow different stages as schematized in Figure 8. The crystallization on a surface from a homogeneous phase is a process controlled by a supersaturation regime. The level of supersaturation depends on the number of molecules impinging the substrates, the temperature of the substrates, and the possible defects or impurities that can act as nucleation sites for the crystal (Figure 8a). These three factors are exactly the variables that we try to control in the methodology of our synthesis. Thus, one of the bases of the model proposed in Figure 8 is the high mobility of the molecules on the substrate (Figure 8ii). This high mobility of the molecules is accomplished under diverse conditions related, among others, to the deposition for certain $T_{substrates}$. These molecules undergo different adsorptions and desorption cycles and move over the surface until they form the nucleus of the crystal at the nucleation sites provided by the substrate grains (Figure 8ii). The development of the crystals by self-assembly of the molecules along the wire axis via strongly directional $\pi-\pi$ interactions (Figure 8iii) permits a mechanism for the growth of 1-D nanostructures (Figure 8iv). The formation of squared and belt nanofibers might depend either on the crystal

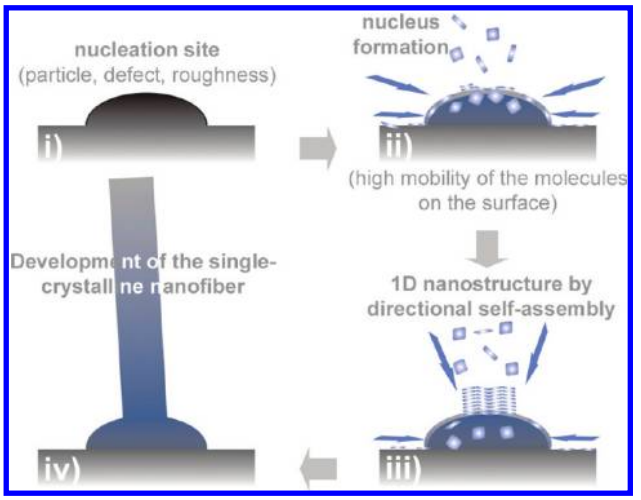

Figure 8. Sketch of the growth mechanism. (i) Metallic particles, rough surfaces, or defects acting as nucleation sites. (ii) Formation of the crystal nuclei by the arrival of a high flux of molecules from the substrate at the nucleation site. (iii) Crystal formation by self-assembly of the molecules. (iv) Development of the single-crystalline 1D nanostructure.

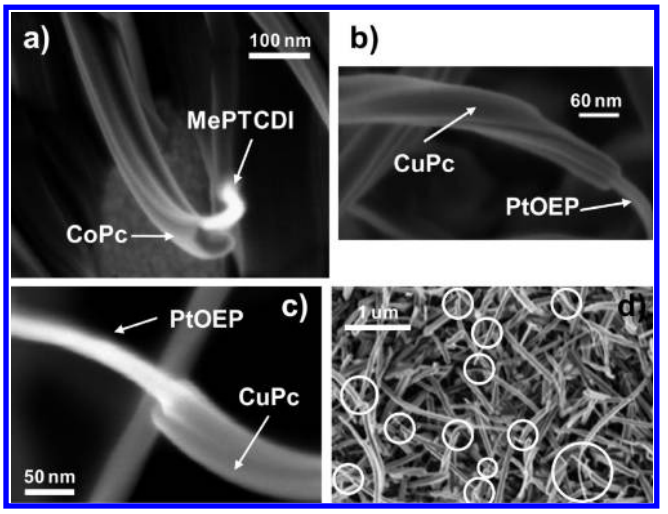

Figure 9. (a) The open core@shell nanofibers formed by a Me-PTCDI inner squared nanofibers wrapped by a CoPc nanobelt on gold. (b, c) SEM micrographs of open core@shell nanofibers formed by an inner thread of PtOEP surrounding by a CuPc nanobelt. (d) Normal SEM micrograph of a high density of these heterostructures grown on silver.

habit or on the nucleus form and size. However, further theoretical analyses are still necessary to fully understand the process.

The Open Core@Shell and the Binary Nanofibers. The generalization of the methodology to different molecules forming 1-D single crystals presents as a grand advantage the option of growing simultaneously nanowires formed by mixtures of different molecular species, i.e., heterostructured nanofibers. Through the numerous experiments carried out under different conditions involving M-OEP, M-Pc, and Me-PTCDI molecules, we have concluded that one of the most important factors for the growth of heterostructured nanofibers is the miscibility of their compounds. In this way, very different 1-D heterostructures have resulted from the combination of miscible molecules (i.e., M-OEP or M-Pc with different metal cations) or nonmiscible molecules (i.e., M-Pc with M-OEP or Me-PTCDI). In this article we present two different types of 1-D heterostructures: the open core@shell

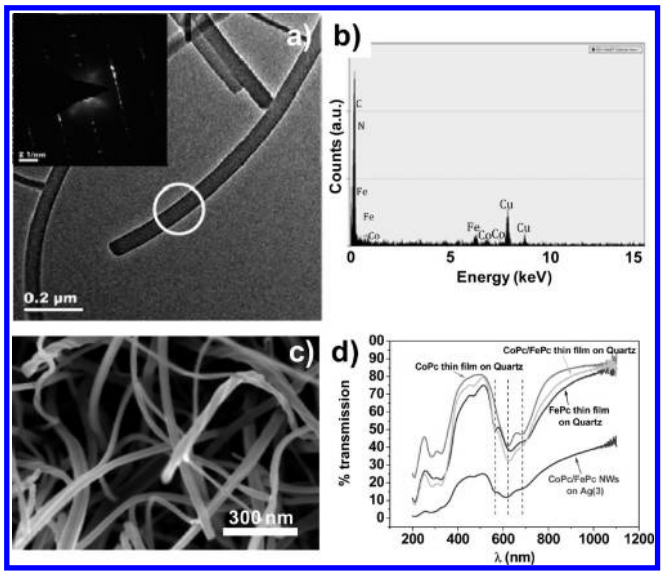

Figure 10. (a) Binary nanofibers formed by CoPc and FePc; the inset shows the corresponding SAED. (b) EDX measured in the TEM of a CoPc + FePc binary nanofiber (65% Fe to 35% Co). (c) Normal view SEM micrograph of the binary CoPc/FePc nanofibers. Both types of fibers, i.e., squared and belt-shaped, are present in the nanofiber thin film. (d) UV−vis transmission spectra of the CoPc/FePc nanowires on Ag(3). The presence in the CoPc/FePc nanofiber thin film of both compounds is clear by comparison with the CoPc thin film, FePc thin film, and CoPc/FePc thin film spectra.

and the binary nanofibers. In the first case, the formation of the nanostructure was achieved by the sequential deposition of two nonmiscible molecules: Me-PTCDI and CoPc (Figure 9a) and PtOEP and CuPc (Figure 9b,c) (see Experimental Section and ref [6i] for the further details). A high density of the open core@shell nanofibers can be achieved as shown in Figure 9d.

The binary nanofibers or nanofibers composed by two M-OEP or two M-Pc were obtained by the controlled simultaneous deposition of the two molecules. In the example of Figure 10 the atomic ratio of the different molecules calculated by EDX analysis (Figure 10b) is approximately 65% Fe to 35% Co (see also the UV−vis spectra in Figure 10d). The composition of the nanofibers is easily controllable by the amount of each molecule reaching the substrate. Both squared binary nanofibers and nanobelts are formed (Figure 10c). Figure S22 shows the growth of PdOEP + PtOEP nanofibers.

Conclusions

In this work we have presented a one-step method for the production of supported single-crystalline nanowires. The generalization of the methodology to planar aromatic molecules that exhibit face-to-face (π-stack) stacking and to different substrates has been accomplished. The different factors controlling the formation of a high density of squared nanofibers and nanobelts have been highlighted. Among such factors, the control of the substrate temperature during the organic molecules deposition permits the nanowires to growth developing different morphologies: cylindrical nanorods, hexagonal nanofibers, squared nanofibers, and nanobelts. Furthermore, a growth mechanism base on a crystallization process has been proposed. This one-step method presents significant advantages for the synthesis of organic semiconductor nanowires such as its simplicity, mild conditions, and relatively low substrate temperature as well as the high

homogeneity and crystallinity of the nanowires synthesized. Besides, for the different molecule species studied in this work, NWs densities as high as 10^9 nanowires cm^{-2} were achieved. Nevertheless, one of the major achievements is the possible growth of heterostructured nanofibers since some of this new 1-D heterostructures can be very interesting in the synthesis of novel n−p nanowires junction for solar energy harvesting applications.[2] In addition, the nanowires grown by this method are in tight contact with the metal particle (cf. Figure 1b) or the semiconductor film at its base (cf. Figure S13) providing a method readily compatible with electrochemical devices. This opens the possibility for the direct incorporation of the 1D structures in functional devices.

Acknowledgment. We thank EU for financial support (PHODYE STREP Project contract no. 033793).

Supporting Information Available: Experimental setup; simulation of electron diffraction pattern for 1-D herringbone structures and additional characterizations. This material is available free of charge via the Internet at http://pubs.acs.org.